

# Improving the Relative Accuracy of the HETGS Effective Area

Herman L. Marshall  
(MIT Kavli Institute)

hermanm@space.mit.edu

## ABSTRACT

I present updates to the HETGS grating efficiencies. When combined with other effective area updates, such as correcting the HRMA Ir-M edge, accounting for contamination, and correcting for a residual Si-K edge, I obtain very good residuals for simple fits to the spectra of many blazars. The updates are somewhat *ad hoc* and the apportionment of the mismatch of the MEG and HEG spectra is determined empirically. The result is that relative uncertainties should now be less than 5% across the HETGS band from 0.5 to 8 keV.

## 1. Overview

The High Energy Transmission Grating Spectrometer (HETGS) has two different grating types that disperse into two independent spectra (Canizares et al. 2005). The medium energy gratings (MEGs) have an energy range of about 0.4-7 keV, depending on the observation parameters, and the high energy gratings (HEGs) have an energy range of about 0.8 to 10 keV. Because they are built into the same structure, the MEG and HEG spectra are obtained simultaneously, facilitating cross calibration even for variable sources. This is an update of the HETG flight calibration paper (Marshall, Dewey, and Ishibashi 2004), which contained some results comparing ACIS-S quantum efficiencies (QEs).

## 2. Data

For this analysis, I used 18 HETGS observations between October, 1999 to June 2005. The sources are listed in Table 1. For most observations, the target's zeroth order was offset by 20'' and the SIM was shifted by -3 mm; exceptions are given in the table. The ACIS focal

Table 1. HETGS Observations used in this Analysis

Target	ObsID	Start Date	Exp. Time	$A$ ph cm <sup>-2</sup> s <sup>-1</sup> keV <sup>-1</sup>	$\Gamma$
3C 273	459 <sup>a</sup>	2000-01-10	38600	0.02534 ± 0.00011	1.666 ± 0.006
3C 273	2463	2001-06-13	26695	0.02389 ± 0.00013	1.731 ± 0.007
3C 273	3456 <sup>b</sup>	2002-06-05	24531	0.02015 ± 0.00013	1.771 ± 0.009
3C 273	3457 <sup>c</sup>	2002-06-05	24849	0.01771 ± 0.00012	1.668 ± 0.009
3C 273	3573	2002-06-06	29680	0.01931 ± 0.00012	1.787 ± 0.008
3C 273	4430	2003-07-07	27750	0.02927 ± 0.00015	1.823 ± 0.007
3C 273	5169	2004-06-30	29863	0.01755 ± 0.00011	1.720 ± 0.008
PKS 2155-304	337 <sup>a</sup>	1999-10-20	38666	0.03762 ± 0.00013	2.642 ± 0.006
PKS 2155-304	1705	2000-05-31	25508	0.03738 ± 0.00017	2.516 ± 0.008
PKS 2155-304	1014	2000-05-31	25508	0.04322 ± 0.00018	2.469 ± 0.007
PKS 2155-304	3167	2001-11-30	29653	0.05498 ± 0.00020	2.730 ± 0.007
PKS 2155-304	3706	2002-11-29	27713	0.01970 ± 0.00013	2.705 ± 0.011
PKS 2155-304	3708 <sup>d</sup>	2002-11-29	26624	0.02577 ± 0.00015	2.750 ± 0.010
PKS 2155-304	5173	2004-11-23	26910	0.02427 ± 0.00015	2.796 ± 0.011
1H1821-63	1599	2001-02-09	101741	0.01450 ± 0.00006	2.021 ± 0.006
Mk 421	1714	2000-05-29	21623	0.01481 ± 0.00009	2.024 ± 0.009
1H1426+428	3568	2001-02-09	103414	0.11968 ± 0.00036	2.400 ± 0.005
1H1426+428	6088	2005-06-25	40385	0.01375 ± 0.00006	1.970 ± 0.006

<sup>a</sup>The ACIS temperature was -110°, the y offset was zero and the SIM z was set to 0 mm.

<sup>b</sup>The SIM z position was set to -5.6 mm.

<sup>c</sup>The SIM z position was set to -8.1 mm, clipping the HEG +1 below 1.4 keV and the MEG -1 below 0.7 keV.

<sup>d</sup>The SIM z position was set to +4.0 mm.

plane temperature was reduced in the middle of January, 2000, so two observations were obtained at  $-110^\circ$ , while the focal plane was  $-120^\circ$  for the remainder.

3C 273 varied by  $\pm 35\%$  about a mean normalization of  $0.0215 \text{ ph cm}^{-2} \text{ s}^{-1} \text{ keV}^{-1}$  (at 1 keV) while PKS 2155-304 varied by up to 70% from a mean of  $0.0321 \text{ ph cm}^{-2} \text{ s}^{-1} \text{ keV}^{-1}$ . The 3C 273 (PKS 2155-304) photon indices varied by  $\pm 0.09$  ( $\pm 0.17$ ) about a mean of 1.734 (2.635). Due to these variations, the residuals from simple power law fits were used to search for spectral features, rather than combining spectra and then fitting.

### 3. Data Reduction

I used IDL-based routines developed independently of the standard *Chandra* data reduction system. The basic approach is nearly identical; I use the same calibration files as provided in the calibration data base except as modified during analysis to investigate or correct systematic errors. The processing begins with level 1 files. The first step is locating zeroth order by fitting Gaussian curves to 1D histograms in sky coordinates. Next, the events are rotated into the detector frame using the average observation roll angle. A  $\pm 3.5''$  rectangular aperture is used to extract source events and background is derived from regions  $7.2\text{--}21.6''$  from the source on both sides. An aperture correction of order 1% is not applied. Accurate CCD energies aren't critical to HETGS analysis, so CCD gains are simply adjusted on a node-by-node basis to keep pulse height centroids within a few percent of the values expected on the basis of the grating dispersion distance – separately for the MEG and HEG.

MEG and HEG events are selected separately using rather wide pulse height windows to accept over 95% of the pulse height distribution. For the MEG, I selected events with ACIS energies within 25% (15%) of the values computed from the +1 (–1) MEG dispersion distance. For the HEG, these values are 12% and 15% for +1 and –1 orders, respectively. Widening the pulse height selection windows to  $\sim \pm 40\%$  did not significantly alter the results, increasing counts by at most a few percent in a few wide energy ranges. Then events in hot CCD columns are eliminated by median filtering in tiled detector coordinates. The HEG (MEG) events are binned at 0.01 (0.005) Å intervals. Data near chip gaps are excised and the effective area is computed using the various system components: HRMA effective areas by shell, grating efficiencies, filter transmission and CCD quantum efficiencies (QEs). Nonstandard treatments are described in the next section.

## 4. Analysis

### 4.1. Correcting for Pileup

The sources were generally very faint during these observations, so pileup effects are generally negligible,  $< 1\%$  at all energies. In one observation, obsID 3568, the pileup effect reached 5% (near 2 keV) and was corrected using the method described by Marshall, Dewey, and Ishibashi (2004). This method seems very effective, *a posteriori*, for brighter sources and in LETGS/ACIS spectra where pileup is more significant.

### 4.2. Correcting for CCD QE Differences

The MEG and HEG dispersion relations differ by a factor of two, so photons of a given energy will be detected at different locations on the focal surface. There are two different CCD types in the detector system and the quantum efficiencies (QEs) are different, so before comparing fluxes at a given energy, the relative QEs of the detectors must be verified. Marshall, Dewey, and Ishibashi (2004) showed that the relative QEs required a correction of up to 10% (see Fig. 1) and that the correction was not time dependent. The BI QEs have now been updated so this correction is no longer necessary (Edgar 2003; Edgar & Vikhlinin 2004).

The FI QEs were multiplied by 0.965 to account for event losses due to cosmic ray blooms; Edgar (2003) reports that this factor should be 0.9632 (no uncertainty given), citing an internal CXC memo by Yousaf Butt. Fig. 2 shows that the ratios of the BI to FI counts are consistent with the new QE models to within  $\pm 5\%$  over the 2-40 Å wavelength range. This plot is not sensitive to systematic errors in the HETGS efficiencies, the HRMA effective area, or absolute ACIS QEs.

The combined residuals from power law spectral fits to AGN observations showed that there were more corrections needed to obtain featureless residuals. Fig. 3 shows that deviations are observed at the Ir-M edge at 2.1 keV and at the Si-K edge at 1.84 keV.

### 4.3. Correcting a Si-K edge Residual

An Si-K edge correction was applied using a high resolution version of the Si-K edge opacity derived from a file provided by Catherine Grant, which is used in the ACIS QE model. The opacity was normalized to unit optical depth just above the Si-K edge at 1.839

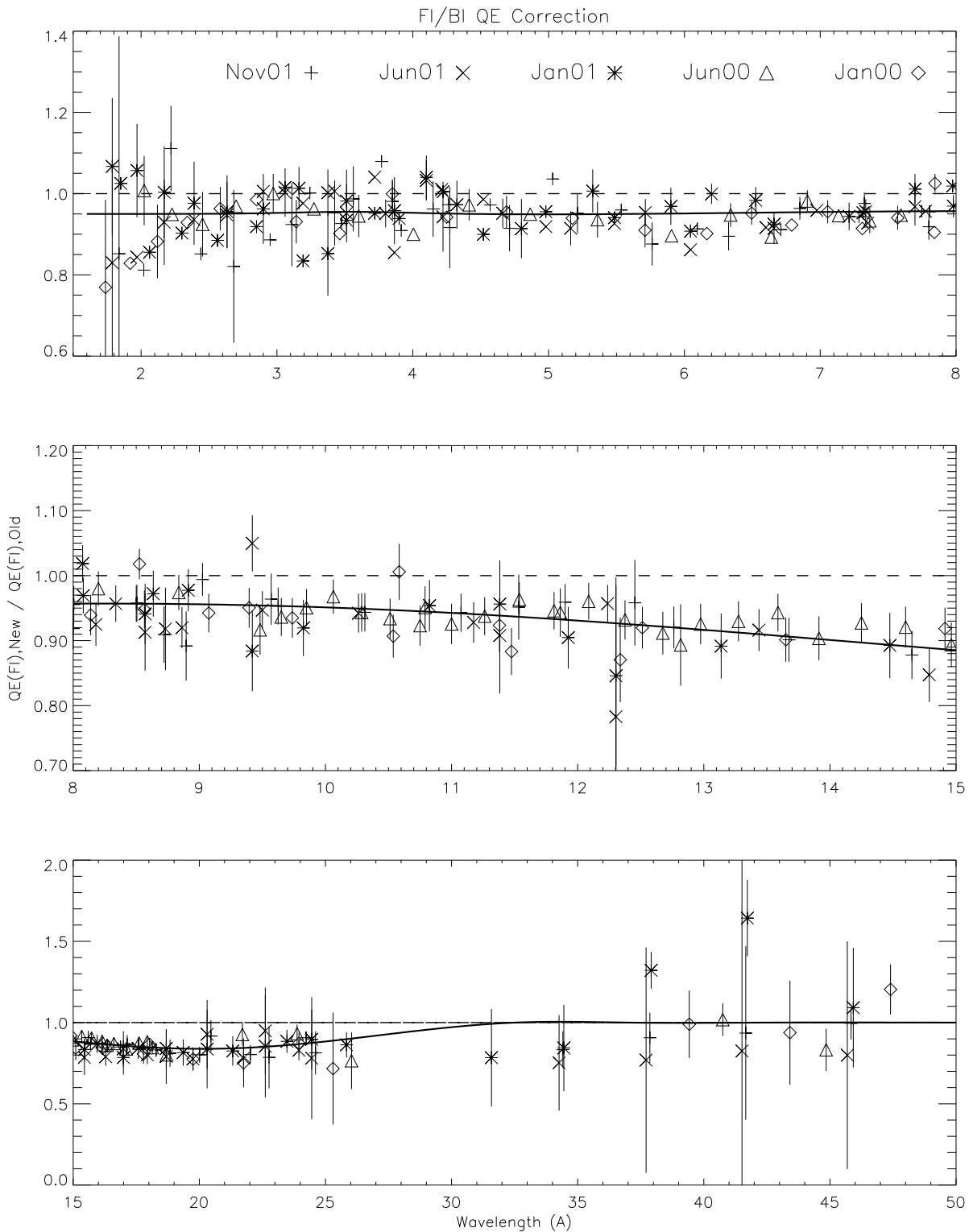


Fig. 1.— The ratio of data from BI CCDs to data from FI CCDs; compare to fig. 7 of Marshall, Dewey, and Ishibashi (2004), which shows the same data but in different time intervals. The ratio is determined using the method given by Marshall, Dewey, and Ishibashi (2004), comparing +1 and –1 orders in LETGS (diamonds and triangles) and HETGS data (crosses and + signs). The values represent the correction to the pre-flight FI QEs that would be needed in order to obtain agreement between the FI and BI data. Edgar (2003) showed that the BI QEs required adjustment below 1 keV, consistent with these data. The dashed line is a polynomial fit to the data that deviates from expectations by over 10% over the 15–25 Å range. At all energies, cosmic ray blooms cause a 3.5% loss of FI events.



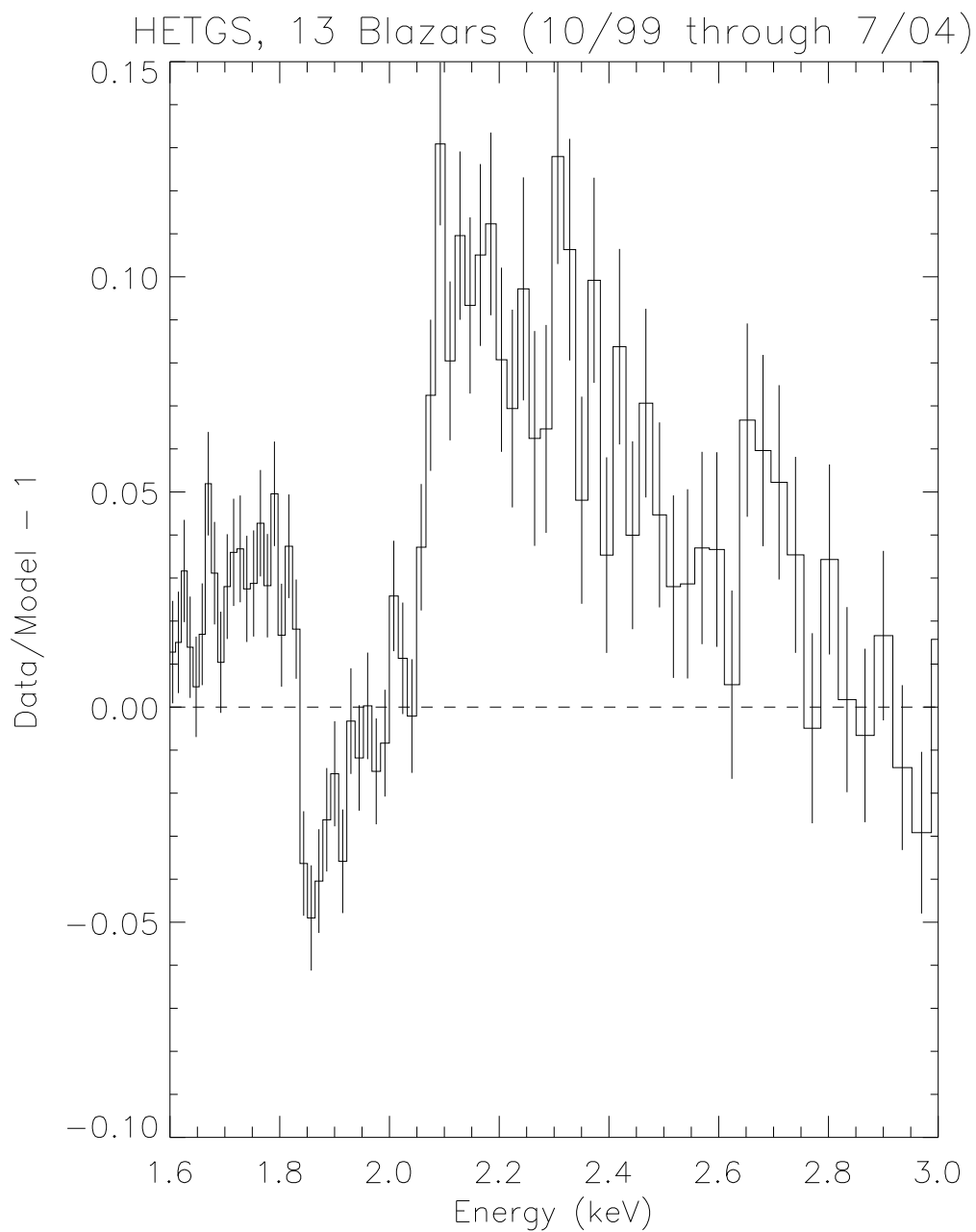


Fig. 3.— Combined residuals from power law fits to 13 blazar spectra. The residuals are binned in equal wavelength intervals. The updated ACIS QE curves were used in the analysis. A significant Si-K edge at 1.84 keV is apparent. The edge at 2.1 keV is coincident with the HRMA Ir-M edge.

keV by extrapolating the Henke constants to this energy, ignoring near edge structure. The correction optical depth was determined to be  $0.063 \pm 0.010$  using a  $\chi^2$  test on the MEG and HEG residuals (fit simultaneously) in the 5.5-8.0 Å region. Local errors in the effective area and spectral fits were eliminated by using a linear continuum model for a total of 3 fit parameters. For  $\nu = 97$  degrees of freedom,  $\chi^2_\nu = 0.975$ . The HRMA Ir-M edge was corrected in a preliminary fashion. The results of the fit are shown in Fig. 4. The form of the QE correction is shown in Fig. 5.

The cause of the Si-K residual is not clear at this time. About 20% of the edge may result from truncating the pulse height distribution. Empirical experimentation with the pulse height selection window indicates that about 1.5% of the events just above the Si-K edge are lost due to low pulse heights. Given that the edge is about 6% deep, the loss of events due to distribution truncation is not the dominant effect. Using selection corrections based on integrals of new, accurate redistribution matrices would help eliminate this source of uncertainty. For the purpose of this analysis, the cause of the edge is irrelevant because there is no Si in the HETG so it shouldn't affect the MEG efficiencies relative to those of the HEG.

#### 4.4. Correcting HRMA Ir-M Edge Residuals

The full set of 18 blazar observations was each fit using a power law model after correcting for ACIS contamination using the so-called “fluffium” model (Dewey 2004; Marshall et al. 2004). The residuals from the HEG and MEG were combined and showed a significant residual that has been attributed to an overlayer of contaminant on the HRMA mirrors. Models of the HRMA reflectivity for a range of overlayer thicknesses from 10 Å to 25 Å were provided by Diab Jerius. Fig. 6 shows how the residuals are improved by replacing the original HRMA effective area. Using data from the 3-8 Å region, the minimum  $\chi^2$  is plotted against the thickness of the overlayer in Fig. 7. The minimum value of the reduced  $\chi^2$  is about 2.0, so there are still some systematic errors remaining. Examining Fig. 6, we see that these are of the order of  $< 3\%$  over this wavelength range. The cause of this residual systematic error is not known.

#### 4.5. Comparing the HEG to the MEG

The HRMA overlayer correction depends on reflection angle, so each HRMA mirror shell has a slightly different correction as a function of energy (see Fig. 8). Thus, uncorrected, there

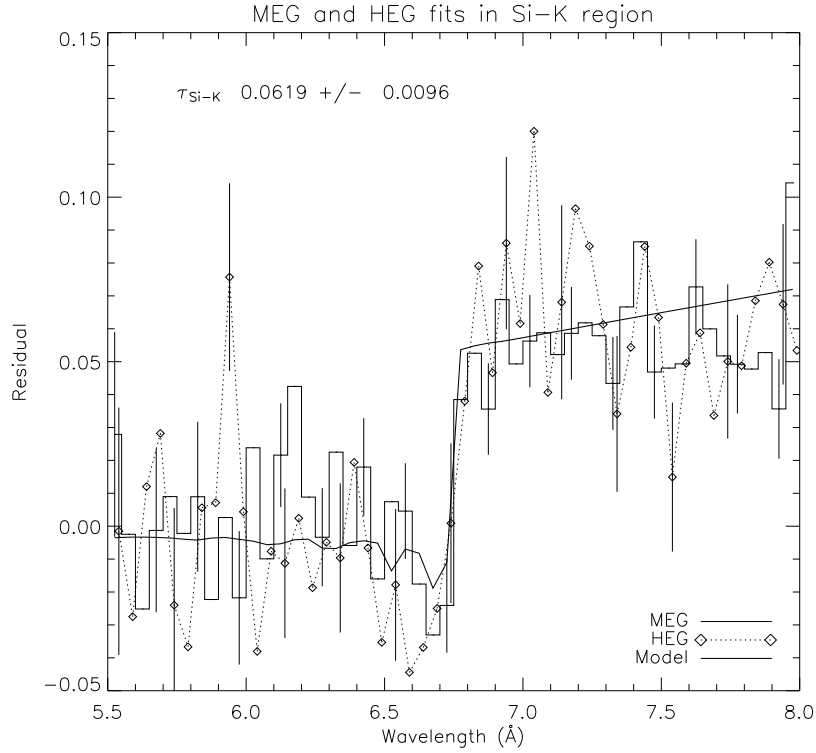


Fig. 4.— Fit to the HEG and MEG residuals in the Si-K region. The MEG and HEG residuals are consistent; because the MEG data involve a BI chip as well as an FI chip while the HEG data only involve FI chips, it is clear that the residual is independent of chip type. The functional form of the edge is shown in Fig. 5, parametrized by a single value: the optical depth extrapolated from high energies using Henke constants (i.e., eliminating near edge absorption structure). The residuals have a slope and normalization offset that were modeled simultaneously. The uncertainty assumes one interesting degree of freedom.

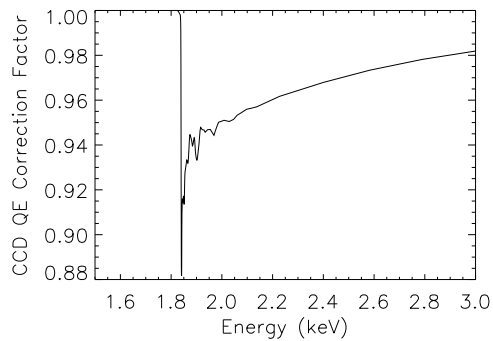


Fig. 5.— Adjustment to the ACIS CCD QEs adopted based on the fit to the data in Fig. 4.

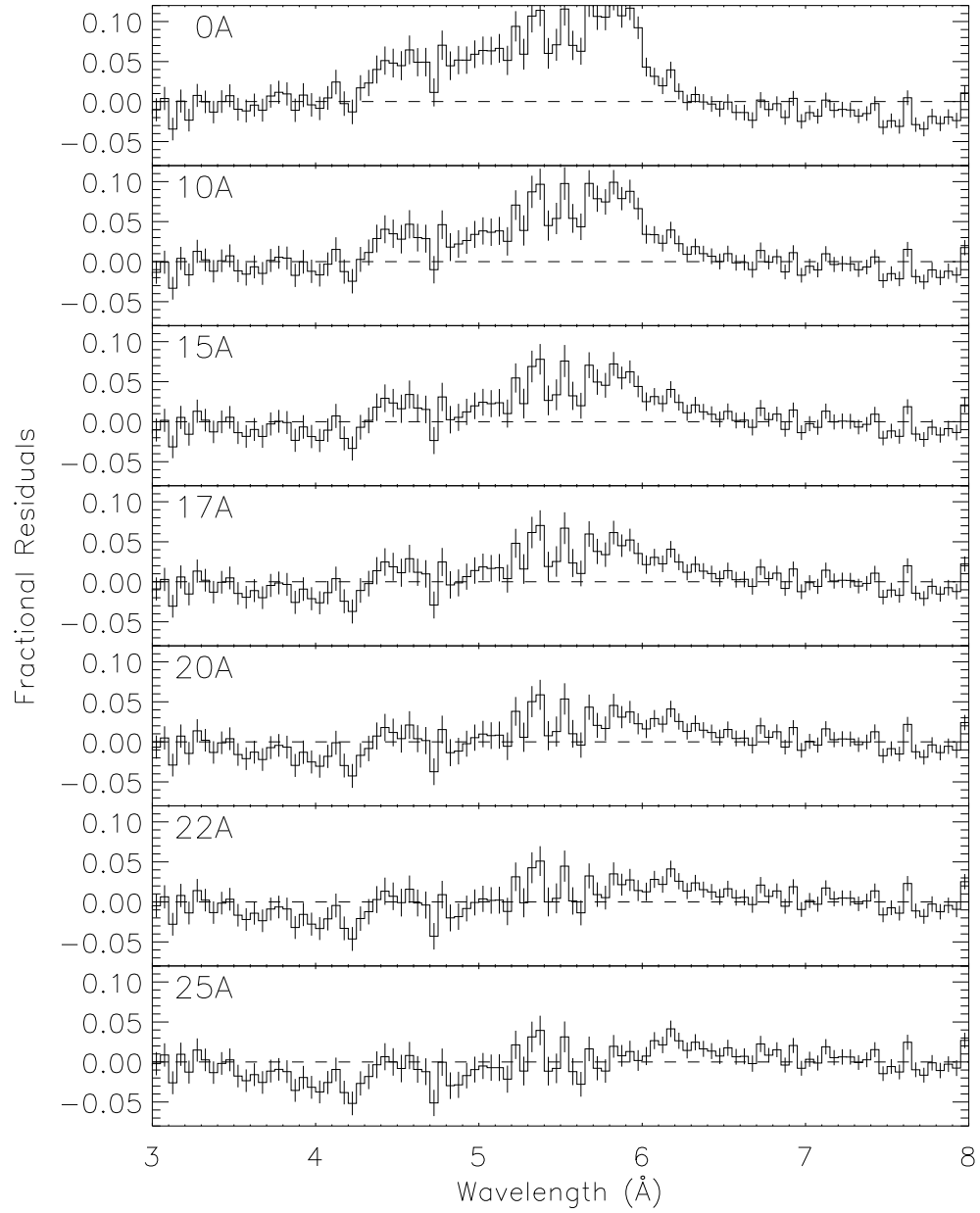


Fig. 6.— Residuals from fits to blazar spectra for different thicknesses of the HRMA contaminant overlayer. The residuals are smoothest for values of the overlayer thickness near 22 Å.

would be a resultant effect upon the fluxes derived from the HEG and MEG. A discrepancy between the HEG and MEG spectra had been noted for many years (e.g. Fang et al. 2001). The discrepancy is determined in a manner similar to that used in comparing BI and FI QEs, by computing the ratio

$$r = \frac{\epsilon^H Q^H \sum_i C_i^M}{\epsilon^M Q^M \sum_i C_i^H} \quad (1)$$

and its statistical uncertainty  $\sigma_r$  over adaptively sized wavelength bins, where  $H$  and  $M$  refer to a grating type (HEG or MEG), index  $i$  refers to a source spectrum number (counting +1 and  $-1$  orders separately, giving 36 spectra for each of MEG and HEG),  $\epsilon$  is the model efficiency of that grating type,  $Q$  is the detector QE for the given wavelength-grating-order combination (using a BI or FI QE as appropriate). Assuming that the grating efficiencies,  $\epsilon$ , are not perfectly known, we assign  $\hat{\epsilon}^H$  and  $\hat{\epsilon}^M$  to represent the *true* efficiencies of these gratings, so that the observed counts in each wavelength bin in the HEG or MEG are given by

$$C_i^H = n_i A Q^H t \hat{\epsilon}^H d\lambda \quad (2)$$

$$C_i^M = n_i A Q^M t \hat{\epsilon}^M d\lambda \quad (3)$$

where  $n_i$  is the source flux in  $\text{ph cm}^{-2} \text{s}^{-1} \text{\AA}^{-1}$ ,  $A$  is the effective area of the HRMA,  $t$  is the observation exposure,  $Q$  is the CCD quantum efficiency (including filter transmission), and  $d\lambda$  is the wavelength interval corresponding to one bin. All quantities are functions of wavelength except  $t$  and  $d\lambda$ .

Thus,  $r$  is a function of *a priori* models of the system effective area and the observed counts, providing a way to compute the correction to the ratio of the grating efficiencies:

$$\frac{\hat{\epsilon}^M}{\hat{\epsilon}^H} = r \frac{\epsilon^M}{\epsilon^H}. \quad (4)$$

The quantity  $r$  is independent of the HRMA effective area and the source model. This ratio is also independent of any absolute errors in the ACIS QE model. However,  $Q$  only drops out of the calculation if there are no errors in one detector QE relative to that of another, because the MEG and HEG data corresponding to the same wavelength are often found on different detectors. CTI corrections are not important but spatially dependent QE variations can affect the ratio. These small QE variations would tend to average out by combining the

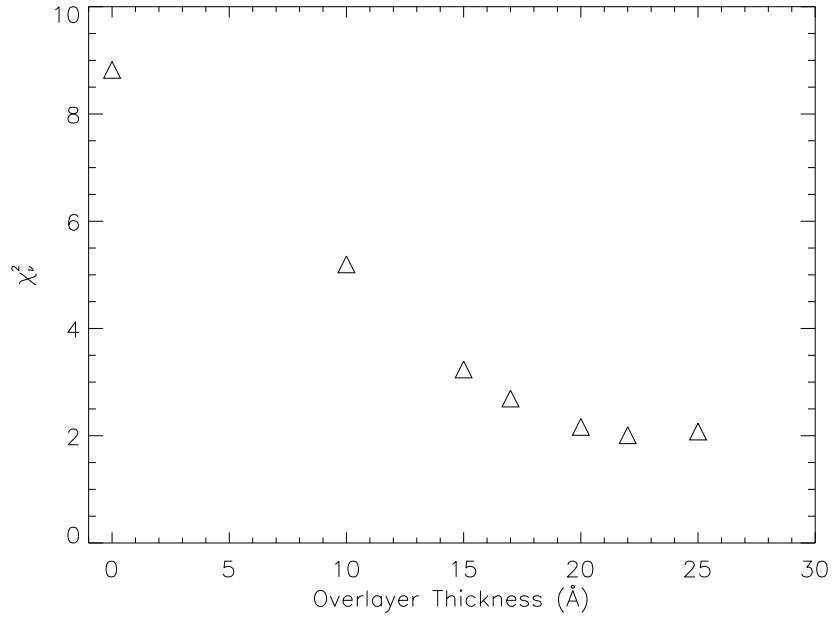


Fig. 7.— Reduced  $\chi^2$  as a function of HRMA contaminant thickness, in Å, for 99 degrees of freedom. The minimum is found at an overlayer thickness of 22 Å.

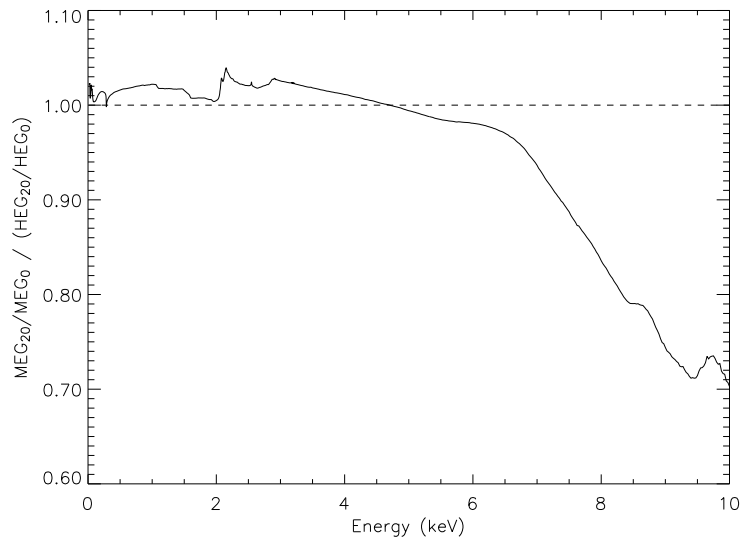


Fig. 8.— Ratio of the changes to the MEG and HEG effective area due to a contamination overlayer of 20 Å on the HRMA. There is an edge about 3% deep at about 2.1 keV at the Ir-M edge. Above 6 keV, the MEG throughput is severely reduced relative to the HEG due to the contaminant.

+1 and –1 orders. The bin wavelength limits,  $\lambda_1$  to  $\lambda_2$ , were limited by  $r/\sigma_r < 50$  and  $\lambda_2 < 1.10\lambda_1$ .

The results are shown in Fig. 9. Also shown in this figure is a fit with a 7th order polynomial to the 1.7-18 Å wavelength range. While the results provide a way to correct the ratio of the grating efficiencies, it is more problematic to determine how to apply this correction because we have one equation – Eq. 4 – but two unknowns:  $\hat{\epsilon}^M$  and  $\hat{\epsilon}^H$ . In the next section, rely on two plausible suppositions: 1- the ratio correction factor is small, so the corrections to the efficiencies should also be small, and 2- that the blazar spectra are smooth and simple.

#### 4.6. Correcting the HEG to the MEG efficiencies: Global Fits

The simplest correction of the HETGS efficiencies is to apply the correction derived in section 4.5 to either the MEG or to the HEG efficiencies. It should be clear if this approach works merely by examining the residuals from pure power law fits to these blazar continua. Fig. 10 shows the results from correcting MEG efficiencies only while Fig. 11 is the corresponding figure when the correction is applied only to the HEG. The HEG and MEG spectra are shown separately for 4 of the 18 observations. It is clear from these figures that the MEG correction is better in the 1-5 keV range but fails below 1.0 keV where the residuals are as large as 20%. By contrast, correcting the HEG only gives relatively good residuals below 1 keV but there is a bump between 1.5 and 3 keV. So, correcting only one of the two grating efficiencies does not provide smooth residuals for PKS 2155-304. The residuals from fits to other observations are similar but are not shown.

Guided by the correlation of the residuals with grating type, I constructed separate efficiency corrections for the HEG and MEG. The MEG-HEG ratio correction was apportioned as a function of wavelength as shown in Fig. 12. There is a transition at 15Å at which the correction factor is attributed predominantly to the MEG at lower wavelengths and to the HEG at higher values. The extrapolations of the polynomial outside the fitted wavelength range at both high and low wavelengths are damped using Gaussians. This correction approach yields significantly improved residuals, as shown in Fig. 13. The residuals for the remaining AGN are shown in Figs. 14, 15, 16, and 17. While there are still some deviations from pure power law spectral fits, there are no specific deviations that appear to be the same across all AGN. These deviations may, instead, be intrinsic to the sources. There have been many reports that the spectral energy distribution (SED) of 3C 273 has a steeper spectrum below 1 keV than above, giving the appearance of a soft excess, as demonstrated in a 30-year average spectrum (Türler et al. 1999). The SEDs of Mk 421 and BL Lac objects from the

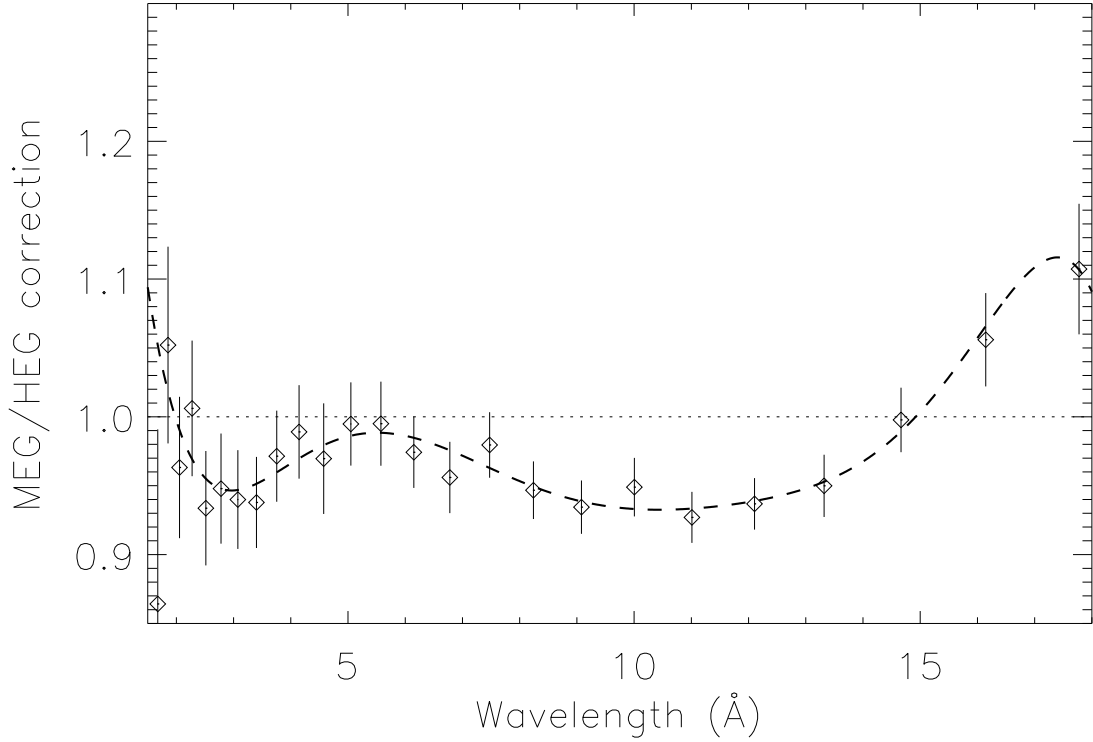


Fig. 9.— Correction required to adjust MEG efficiencies to provide agreement between the MEG and HEG fluxes. Data from 18 blazar observations were adaptively binned to obtain 2% uncertainties but requiring bins to be larger than  $0.10\lambda$ . The ratios were computed after correcting for HRMA contamination and BI/FI QE differences. The thick dashed line is a fit with a 7th order polynomial to the 1.7-18 Å wavelength range. This correction is allocated partly to the MEG and partly to the HEG efficiencies, as described in section 4.6.

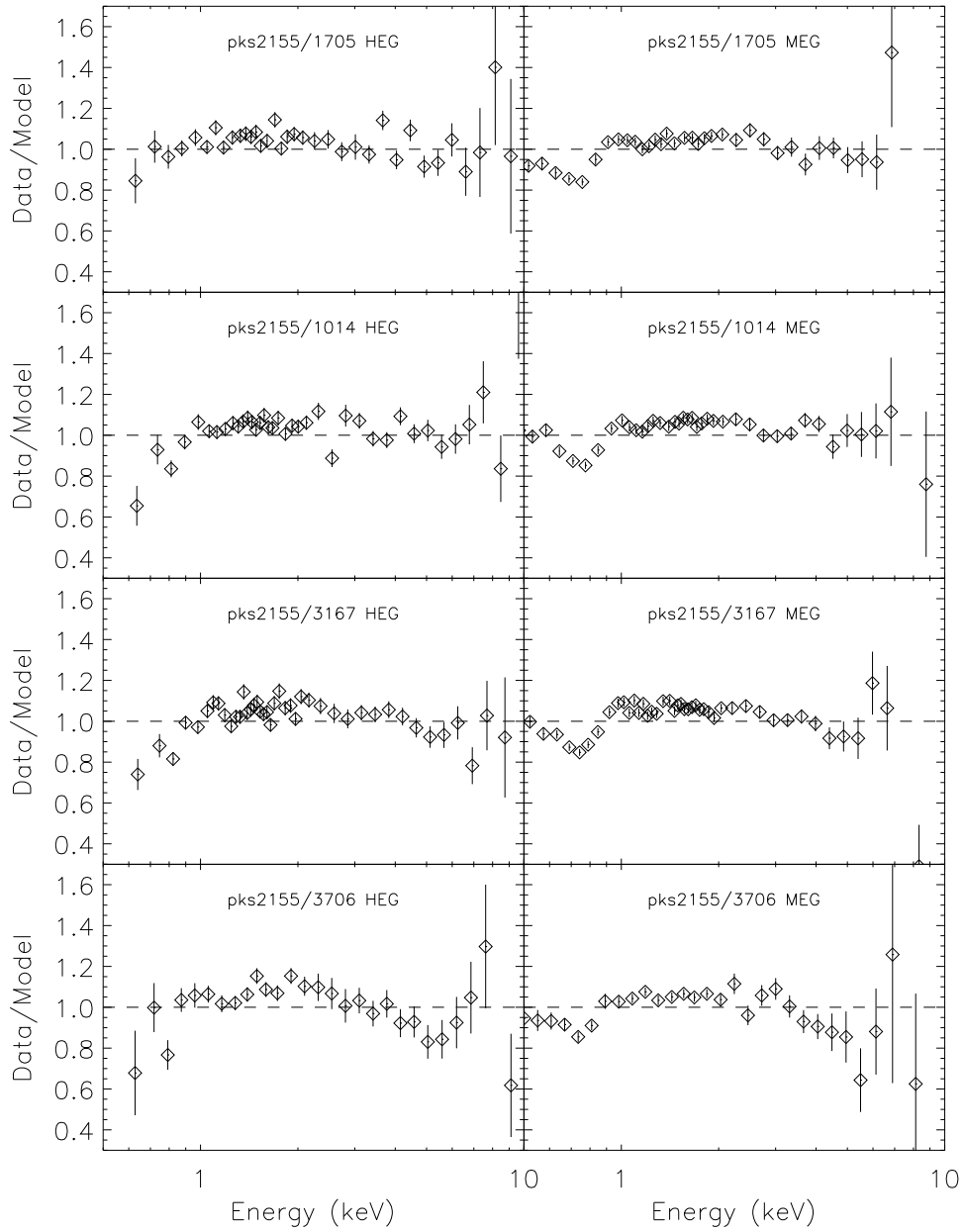


Fig. 10.— Residuals from fits to several observations of blazars when fixing only the MEG efficiencies.

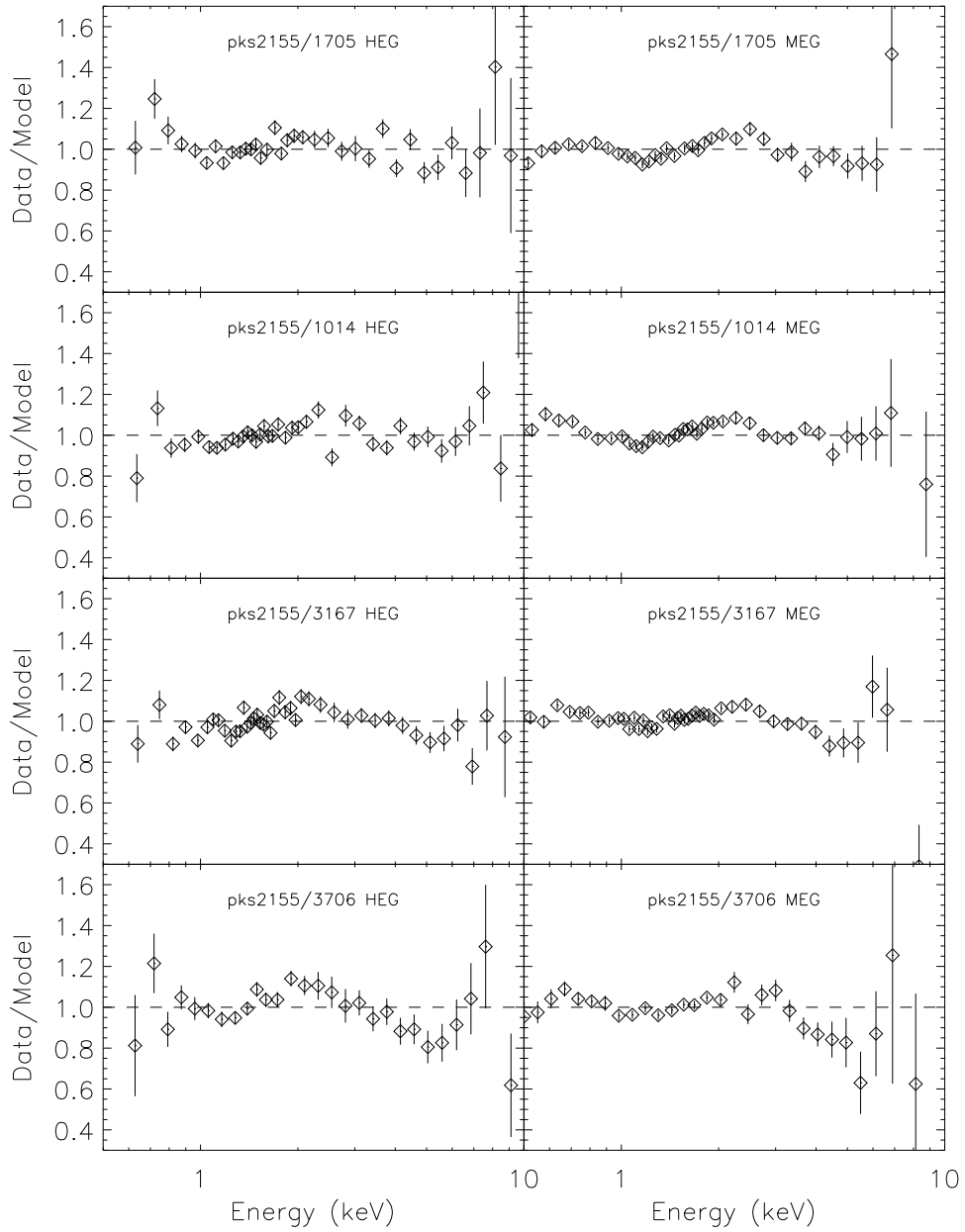


Fig. 11.— Residuals from fits to several observations of blazars when fixing only the HEG efficiencies.

Einstein Slew Survey show steepening spectra (Massaro et al. 2004; Perlman et al. 2005), so, by implication, PKS2155-304 and 1H1426+428 are also likely to show downward deviations at the high and low energy ends of the HETGS spectra, as generally observed.

## 5. Conclusions

Substantial systematic errors at the  $\sim 10\%$  level attributable to the CCDs, the HRMA, and the HETGS efficiencies have been removed reasonably well using these blazar observations. The remaining errors appear to be less than 5% over the 0.5 to 8 keV range.

## REFERENCES

- Canizares, C.R., et al., 2005, PASP, 117, 1144 (astro-ph/0507035).
- Dewey, D., 2004, <http://space.mit.edu/HETG/technotes/contam/twolevel.html>.
- Edgar, R.J., 2003, Chandra X-ray Center memo dated 6/9/2003, [http://cxc.harvard.edu/cal/Acis/Cal\\_prods/qe/ACIS\\_QE\\_0\\_S23.ps](http://cxc.harvard.edu/cal/Acis/Cal_prods/qe/ACIS_QE_0_S23.ps).
- Edgar, R.J., & Vikhlinin, A.A., 2004, Chandra X-ray Center memo dated 8/11/2004, [http://cxc.harvard.edu/cal/Acis/Cal\\_prods/qe/qe\\_memo.ps](http://cxc.harvard.edu/cal/Acis/Cal_prods/qe/qe_memo.ps).
- Fang, T., Marshall, H. L., Bryan, G. L., & Canizares, C. R. 2001, ApJ, 555, 356
- Marshall, H.L., Tennant, A., Grant, C., Hitchcock, A.P., O’Dell, S., and Plucinsky, P.P., 2004, Proceedings SPIE, 5165, 497 (astro-ph/0308332).
- Marshall, H.L., Dewey, D., and Ishibashi, K., 2004, Proceedings SPIE, 5165, 457 (astro-ph/0309114).
- Massaro, E., Perri, M., Giommi, P., & Nesci, R. 2004, A&A, 413, 489
- Perlman, E. S., et al. 2005, ApJ, 625, 727
- Türler, M., et al. 1999, A&AS, 134, 89

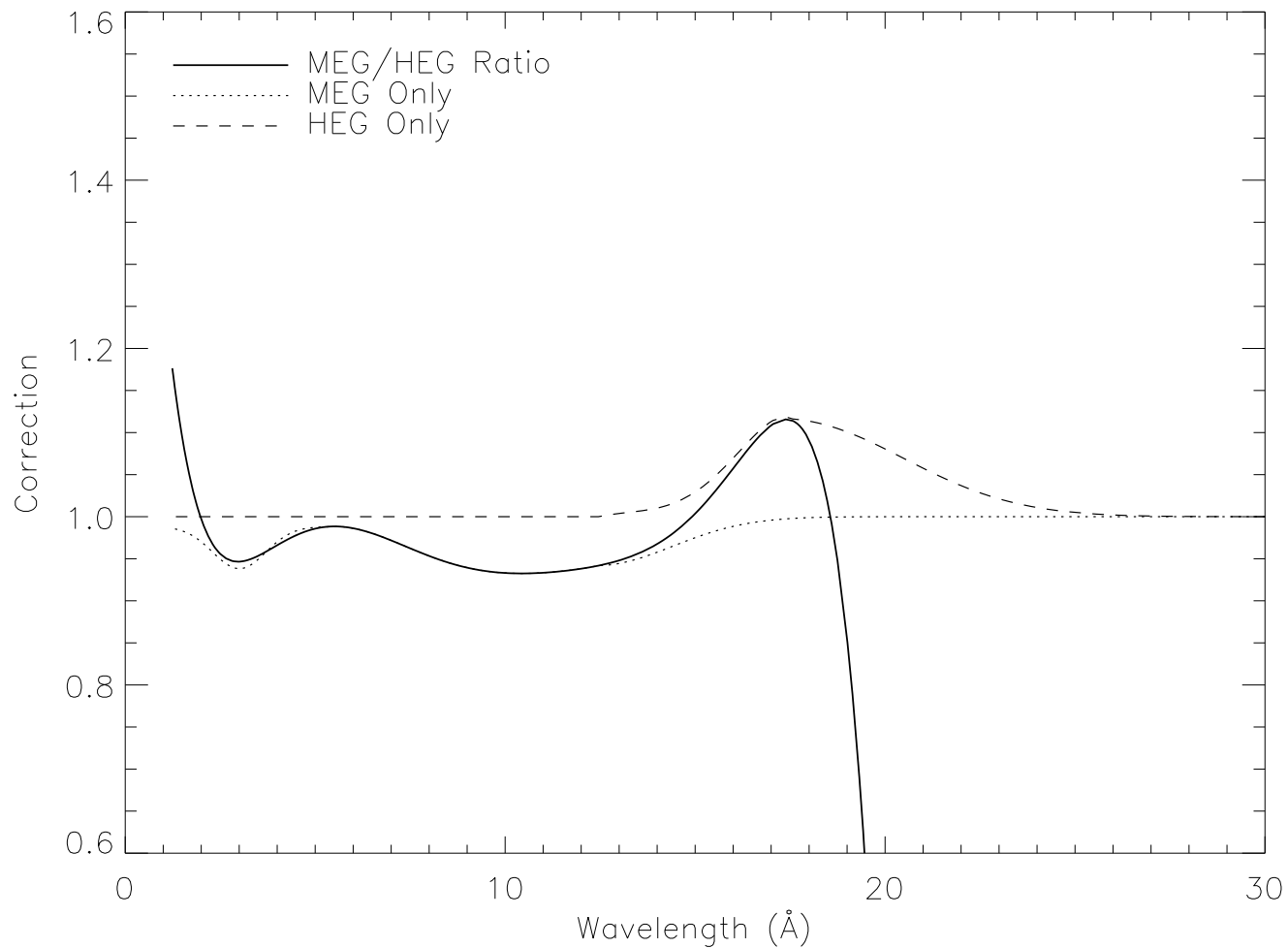


Fig. 12.— Apportioning the MEG-HEG ratio correction as a function of wavelength. The solid curve shows the correction factor as modeled by a polynomial, taken from Fig. 9. There is a transition at 15 Å at which the correction factor is attributed predominantly to the MEG at lower wavelengths and to the HEG at higher values. The extrapolations of the polynomial outside the fitted wavelength range at both high and low wavelengths are damped using Gaussians.

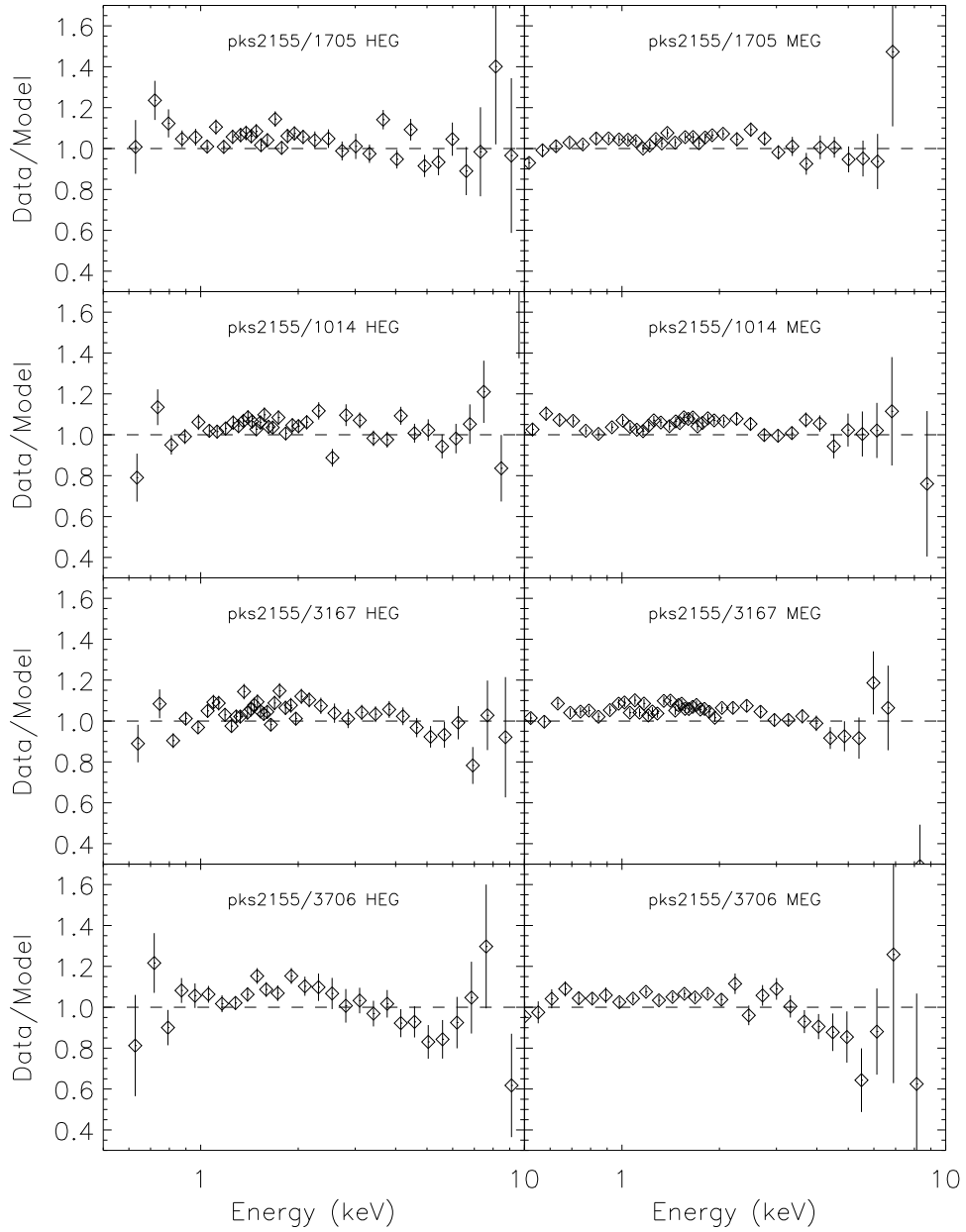


Fig. 13.— Residuals from fits to several observations of blazars when fixing both the HEG and MEG efficiencies according to the prescription given in Fig. 12.

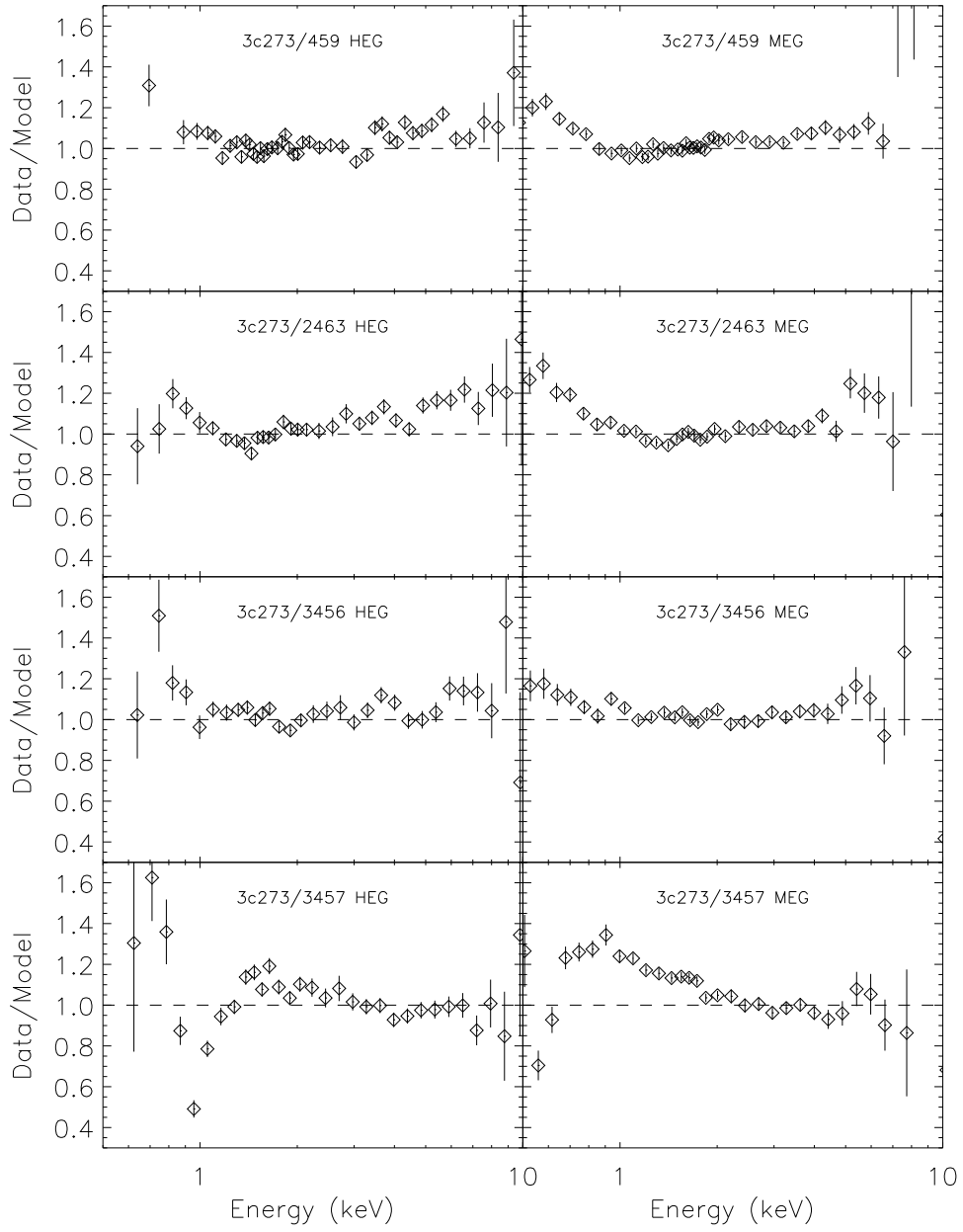


Fig. 14.— Same as Fig. 13 except for a different set of blazar observations. The large deviations in obsID 3457 below 1.4 keV in the HEG and below 0.7 keV in the MEG result from clipping at the edge of the subarray due to the SIM z position (see table 1).

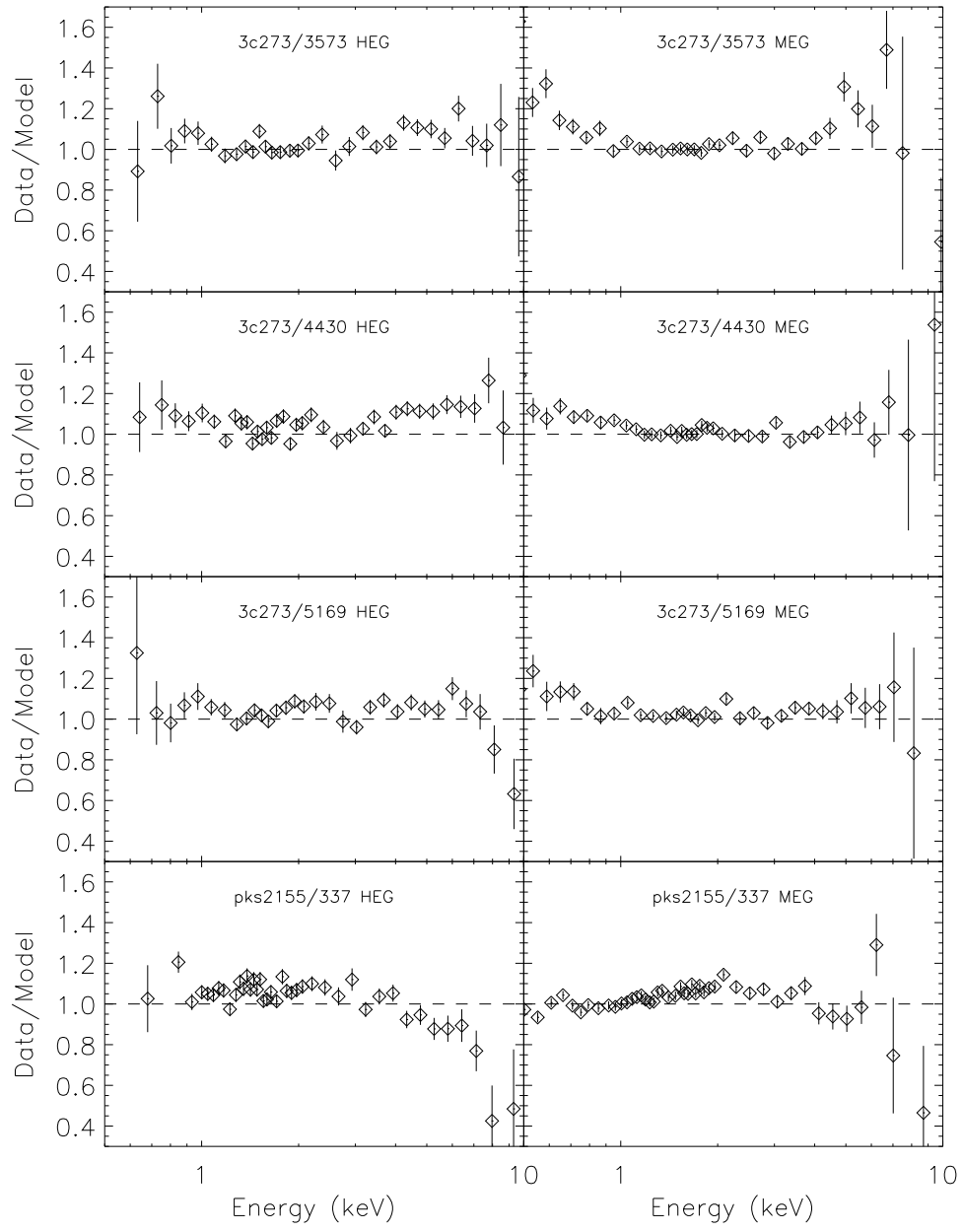


Fig. 15.— Same as Fig. 13 except for a different set of blazar observations.

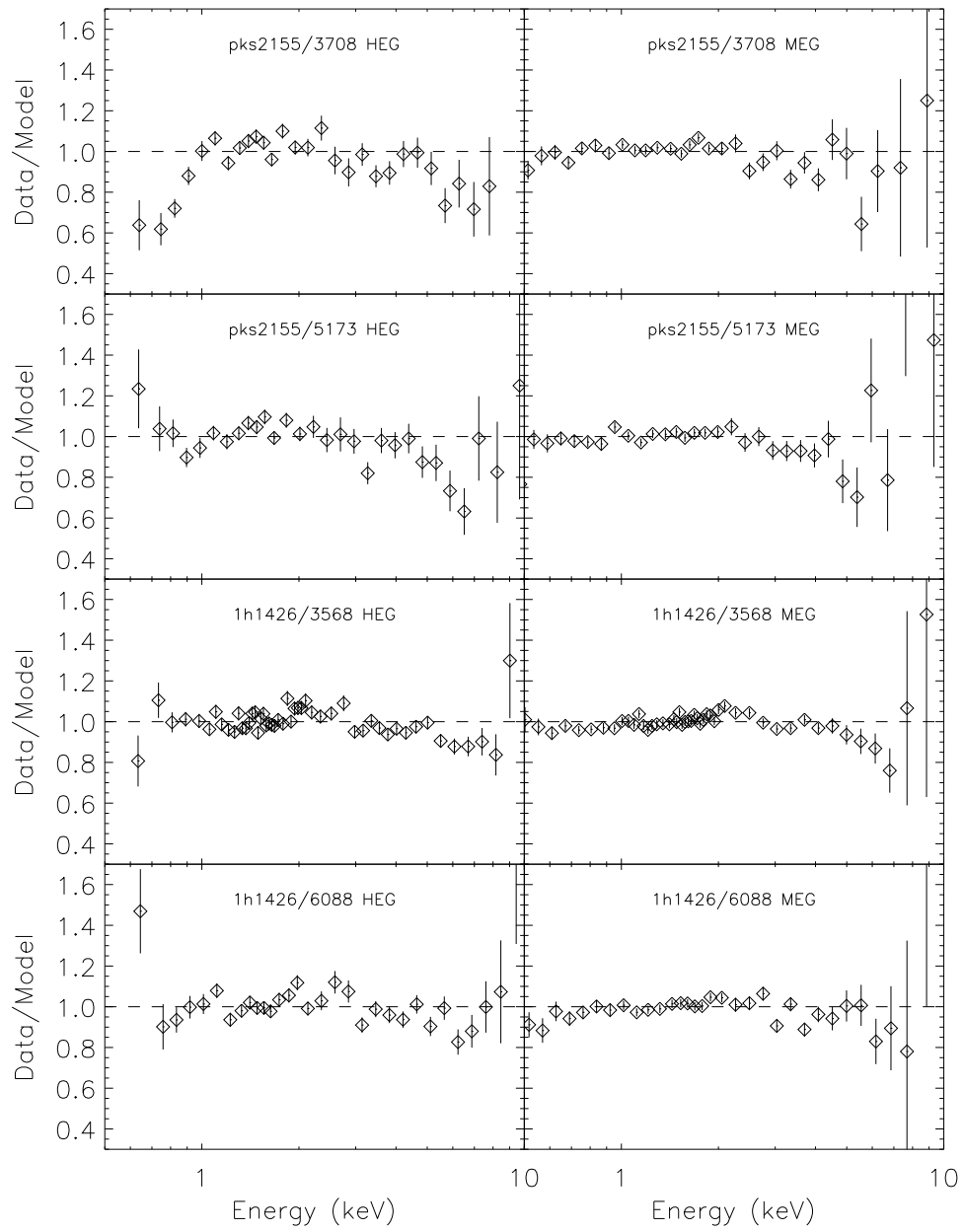


Fig. 16.— Same as Fig. 13 except for a different set of blazar observations.

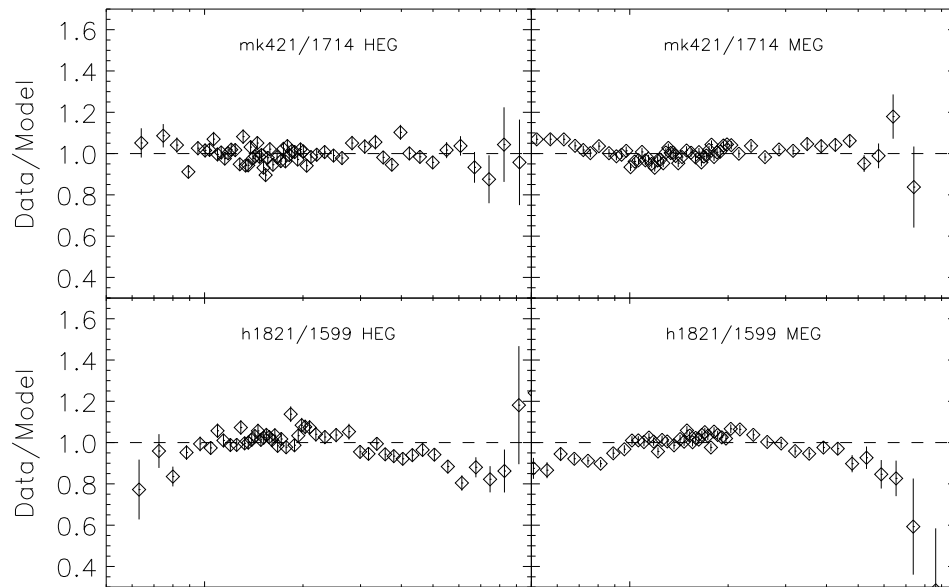


Fig. 17.— Same as Fig. 13 except for a different set of blazar observations.